Journal of Zhejiang University-SCIENCE A (Applied Physics & Engineering) 2025 26(6):525-539
www.jzus.zju.edu.cn; www.springer.com/journal/11582
E-mail: jzus_a@zju.edu.cn

Research Article
https://doi.org/10.1631/jzus.A2300285

Performance of a hybrid system with a semi-submersible wind platform and annular wave-energy converters

Binzhen ZHOU[1], Yu WANG[1], Zhi ZHENG[1], Peng JIN[1,2]✉, Lei WANG[1], Yujia WEI[3,4]

[1]*School of Civil Engineering and Transportation, South China University of Technology, Guangzhou 510641, China*
[2]*School of Marine Science and Engineering, South China University of Technology, Guangzhou 511442, China*
[3]*Department of Naval Architecture, Ocean and Marine Engineering, University of Strathclyde, Glasgow G4 0LZ, UK*
[4]*Division of Energy and Sustainability, Cranfield University, Cranfield MK43 0AL, UK*

Abstract: Installing annular wave-energy converters (WECs) on the columns of floating wind platforms in the form of a coaxial-cylinder provides a convenient means of integration. Extant coaxial-cylinder-type wind-wave hybrid systems are mostly based on single-column platforms such as spars ('single coaxial-cylinder hybrid system' hereafter). Systems based on multiple-column platforms such as semi-submersible platforms ('multiple coaxial-cylinder hybrid systems' hereafter) are rarely seen or studied, despite their superiority in wave-power absorption due to the use of multiple WECs as well as in dynamic stability. This paper proposes a novel WindFloat-annular-WEC hybrid system, based on our study investigating its dynamic and power features, and optimizing the geometry and power take-off of the WECs. Our results show that the dynamic and power features of a multiple coaxial-cylinder hybrid system are different from those of a single coaxial-cylinder hybrid system, so the same optimization parameters cannot be directly applied. Flatter annular WECs absorb slightly more power in a wider wave-period range, but their geometry is confined by limitations in installation and structural strength. The overall effect of an oblique incident wave is greater intensity in the motions of the hybrid system in yaw and the direction perpendicular to propagation, although the difference is small and may be negligible.

Key words: Semi-submersible wind platform; Wave energy; Annular wave-energy converter (WEC); Power performance; Motion

1 Introduction

Ocean-wave energy is regarded as a promising renewable energy resource and a possible substitute for traditional fuels (Said and Ringwood, 2021). It has been widely explored in recent years, as reflected by numerous new wave-energy conversion technologies (Zhang YX et al., 2021; He et al., 2023). Despite the abundance of wave-energy converters (WECs) in theoretical studies, model tests, and sea trails, their practical application is still hindered by their low technology readiness level (TRL), which leads to high construction and maintenance costs (Penalba and Ringwood, 2019) for multivarious waves in realistic ocean (Wang et al., 2023; Zhou et al., 2023a). To reduce the cost, the prevailing approach is to install WECs on existing coastal and offshore infrastructures to utilize their foundations, moorings, maintenance, and power grids (He et al., 2013, 2019; Zhang HM et al., 2021a, 2021b; Zhou et al., 2022b, 2023c). Among such hybrid systems, those consisting of floating offshore wind turbines and WECs provide the most effective scenario for co-located extraction of multiple sources of ocean renewable energy, exploiting the coherent strong winds and high waves in deep seas (Chen et al., 2017; Clemente et al., 2021). Innovative projects have been supported by the government and industrial community to prompt the development of co-located offshore renewable energy extraction (Jeffrey and Sedwick, 2011; Lu et al., 2014), and many wind-wave hybrid systems have been proposed (Kamarlouei et al., 2020; Gaspar et al., 2021; Ghafari et al., 2021; Si et al., 2021).

Of the various hybrid systems, the coaxial-cylinder type is the most widely accepted. In most of these

✉ Peng JIN, jinpeng@scut.edu.cn
Binzhen ZHOU, https://orcid.org/0000-0003-0821-5033
Peng JIN, https://orcid.org/0000-0002-2010-1840

Received May 28, 2023; Revision accepted Sept. 5, 2023; Crosschecked May 20, 2024; Online first July 22, 2024

systems, annular WECs are installed on the leg columns of the foundation of offshore wind platforms through, for example, a clamp mechanism (Muliawan et al., 2012). The annular WEC can then slide along the column and generate wave power through a linear permanent magnet generator (Faiz and Nematsaberi, 2017) power take-off (PTO) driven by the relative heave motion between the WEC and the column. Such hybrid systems use existing columns as an installation foundation, which is convenient since no additional modification of the structure is required. Representative designs are the spar-torus combination (STC) (Wan et al., 2016, 2020; Cheng et al., 2019; Lerch et al., 2019), tension leg platform (TLP)-wind turbine (WT)-WEC combination (TWWC) (Ren et al., 2020), and monopile-WT-WEC combination (MWWC) (Ren et al., 2019). In these three systems, the floating or fixed foundation of the platform has a single cylindrical column, which means they can be appropriately called single coaxial-cylinder hybrid systems. The design was originally inspired by a coaxial-cylinder WEC Wavebob (Muliawan et al., 2013). Therefore, the annular WECs used in these hybrid systems were directly borrowed from the configuration of the outer cylinder of the Wavebob. The dynamic and power features of the single coaxial-cylinder hybrid systems have been extensively investigated in previous studies through numerical simulations and model tests, providing quite a bit of useful guidance for design and operation in both mild and extreme sea states.

Annular WECs are not only suitable for integration into single-column offshore wind platforms such as spars. In fact, among floating offshore wind platforms employing three prevalent types of floating foundation (spar, tension-leg platform, and semi-submersible platform), semi-submersible foundations that contain multiple columns account for over 90% of the platforms in service (Wu et al., 2019), providing a much wider basis of choice for integration of annular WECs. WindFloat (Roddier et al., 2010) is a representative platform. It was developed in 2003 by the offshore engineering consulting company Marine Innovation & Technology (MI&T) as a foundation for multimegawatt offshore wind turbines from different manufacturers. It aims to provide acceptable static and dynamic motion for the operation of large wind turbines, while limiting expensive offshore installation and maintenance procedures in deep-sea areas (Jensen and Mansour, 2006; Jonkman and Sclavounos, 2006; Joensen et al., 2007). Three annular WECs can be installed on the three columns of WindFloat, one on each. Such a configuration is referred to as a multiple coaxial-cylinder hybrid system hereafter, to distinguish it from single coaxial-cylinder hybrid systems.

Compared with single coaxial-cylinder hybrid systems, multiple coaxial-cylinder hybrid systems may offer higher wave-power generation through the use of multiple annular WECs, and the motion can be more stable because of the use of a semi-submersible foundation instead of a spar. Despite these merits, multiple coaxial-cylinder hybrid systems are rarely seen and their dynamic features and power performance are poorly understood, hindering analysis and optimization. The reasons and specific gaps are as follows. The more complex configuration of the multiple coaxial-cylinder hybrid systems causes difficulties in the analysis of their dynamic and power features. Data from single coaxial-cylinder hybrid systems may be referred to, but the applicability is uncertain because the dynamic and power features of the two types of hybrid systems can be quite different. Turning to the optimization of annular WECs, in previous studies of single coaxial-cylinder hybrid systems, the geometry of the WEC was primarily based on the Wavebob device, and the PTO parameters were assigned randomly chosen values. The optimization method proposed by Jin et al. (2019) for a coaxial-cylinder WEC could be useful, but it may or may not be suitable for a configuration with multiple annular WECs. These gaps are filled in this study. We propose a novel WindFloat-annular-WEC hybrid system. The dynamic and power features of the multiple coaxial-cylinder hybrid system not covered in previous studies are unfolded here, showing that they are indeed quite different from those in a single coaxial-cylinder hybrid system. The dimensions and PTO damping of the annular WECs are also optimized based on our findings. The influence of incident-wave direction was ignored in previous studies as a single coaxial-cylinder hybrid system is insensitive to this factor. However, it is emphasized in this paper as we found that the stability of a multiple coaxial-cylinder hybrid system can be affected by its centrosymmetric configuration.

The rest of the paper is structured as follows. In Section 2, the configuration of the WindFloat-annular-WEC hybrid system is described and the key parameters of the floating foundation of the platform are provided. In Section 3, the constrained dynamics and power absorption that govern the hybrid system are mathematically modelled and validated against published results. In Section 4, the dynamic and power absorption features of the annular WECs are analyzed and the dimensions of the annular WECs optimized. The influence of incident-wave direction on the power performance and motion of the optimized hybrid system is also investigated.

2 Configuration of the WindFloat-annular-WEC hybrid system

2.1 Hybrid system

The proposed wind-wave hybrid system consists of a WindFloat offshore wind platform and three identical annular WECs (Fig. 1). WindFloat consists of an equilateral triangular semi-submersible floating foundation and a mooring system. The floating foundation has three cylindrical columns, each equipped with a heave plate to dampen the motion of the platform. The annular WEC, whose geometry is characterized by its inner radius r, outer radius R, and draft d, is installed on the column like a sleeve on a shaft. As the radius of the column is 5.35 m, the inner radius of the annular WEC is preset to 5.5 m to leave a narrow gap between the two. A linear permanent magnet generator is embedded in the gap between the annular WEC and the column as a direct-drive PTO. The motions of the annular WEC in the other five degrees of freedom (DOFs) are restricted by some mechanics, and only relative heave motion is allowed. Wave power is absorbed through the relative heave motion between the platform and the annular WEC.

2.2 Platform and mooring system

The key parameters of the WindFloat offshore wind platform are given in Table 1. The layout of the four catenary mooring cables is illustrated in Fig. 1 and the key parameters can be found in reference (Zhou et al., 2023b). To adopt the frequency-domain wave-structure interaction method in the hybrid system simulation, we made the mooring system equivalent to a matrix-mooring stiffness (Zhou et al., 2023b) calculated by the open-source tool Mooring Analysis Program (MAP) (Masciola et al., 2014).

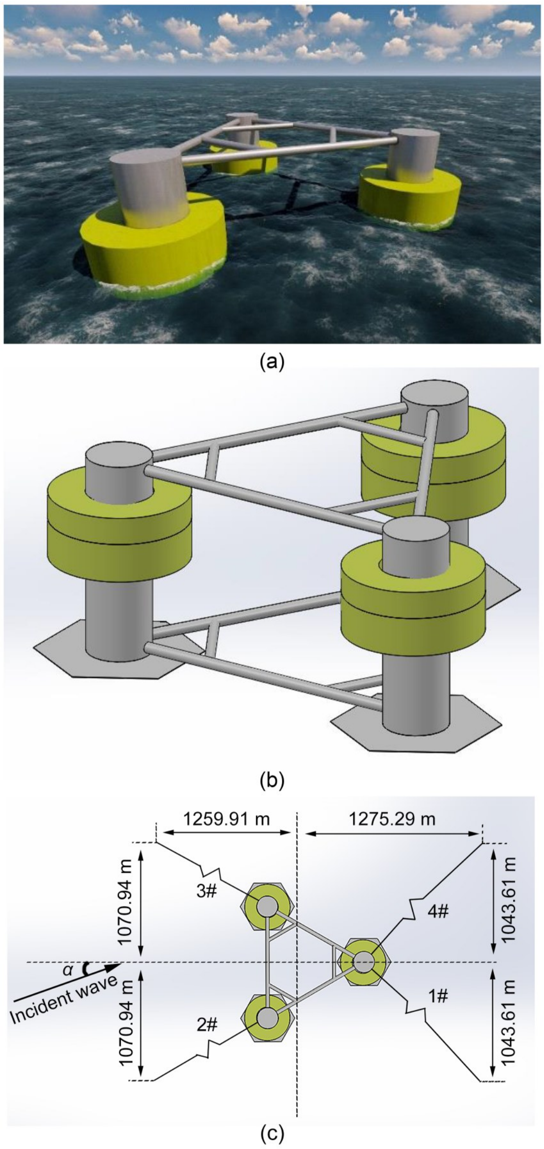

Fig. 1 WindFloat-annular-WEC hybrid system: (a) 3D rendered sketch; (b) side view; (c) top view. α is the incident-wave angle

Table 1 Detailed dimensions of WindFloat platform (Roddier et al., 2010)

Parameter	Value
Column diameter (m)	10.7
Pontoon diameter (m)	1.8
Column center-to-center distance (m)	56.4
Height of hexagonal damping plate (m)	0.1
Length of heave-plate edge (m)	13.7
Total platform height (m)	33.6
Operating draft (m)	22.9
Displacement (t)	7105
Center of gravity (m)	17.9

3.1 Constrained motion equation

The WAFDUT numerical package used in this analysis, developed by the Dalian University of Technology, China, is based on the potential flow theory of linear waves and the higher-order boundary element method (HOBEM). Its wave-structure interaction fundamentals can be readily referred to in reference (Teng and Taylor, 1995). The WAFDUT numerical package can simulate the hydrodynamics of thin heave plates such as those in the WindFloat. Here, we highlight the constrained motion equation of the hybrid system and the wave-power absorption equation.

Identical PTO is applied to all three annular WECs and is simplified as linear damping, as in many previous studies (Zhang HM et al., 2020a, 2020b; Zhou et al., 2022a). The matrix form of the constrained motion equation of the hybrid system is

$$[-\omega^2(\boldsymbol{M}+\boldsymbol{a})-\mathrm{i}\omega(\boldsymbol{b}+\boldsymbol{b}_{\mathrm{PTO}}+\boldsymbol{b}_{\mathrm{vis}})+\boldsymbol{k}_{\mathrm{r}}+\boldsymbol{k}_{\mathrm{m}}]\boldsymbol{\xi}=\boldsymbol{F}_{\mathrm{wave}}+\boldsymbol{F}_{\mathrm{c}}, \tag{1}$$

where i is the imaginary unit, and ω is the angular frequency of the incident wave. $\boldsymbol{M}$, $\boldsymbol{a}$, $\boldsymbol{b}$, $\boldsymbol{b}_{\mathrm{PTO}}$, $\boldsymbol{b}_{\mathrm{vis}}$, $\boldsymbol{k}_{\mathrm{r}}$, and $\boldsymbol{k}_{\mathrm{m}}$ are all 24×24 matrices of mass, added mass, radiation damping, PTO damping, fluid viscous damping correction of the platform, hydrostatic restoration coefficient, and mooring stiffness of the system, respectively. $\boldsymbol{\xi}$, $\boldsymbol{F}_{\mathrm{wave}}$, and $\boldsymbol{F}_{\mathrm{c}}$ are the vectors of displacement, wave excitation force, and constraint force, respectively. $\boldsymbol{M}$, $\boldsymbol{a}$, $\boldsymbol{b}$, $\boldsymbol{k}_{\mathrm{r}}$, and $\boldsymbol{F}_{\mathrm{wave}}$ are all calculated in the WAFDUT numerical package. In the matrix of PTO damping $\boldsymbol{b}_{\mathrm{PTO}}$, the values of part of its elements are $b_{\mathrm{PTO},3,3}=b_{\mathrm{PTO},9,9}=b_{\mathrm{PTO},15,15}=b_{\mathrm{PTO}}$ and $b_{\mathrm{PTO},3,21}=b_{\mathrm{PTO},9,21}=b_{\mathrm{PTO},15,21}=b_{\mathrm{PTO},21,3}=b_{\mathrm{PTO},21,9}=b_{\mathrm{PTO},21,15}=-b_{\mathrm{PTO}}$, with b_{PTO} representing the value of the PTO damping. The values of the other elements in $\boldsymbol{b}_{\mathrm{PTO}}$ are all 0. $\boldsymbol{b}_{\mathrm{vis}}$ is obtained without considering the couplings between motions in different DOFs or between different floating bodies through the method proposed by Zhou et al. (2023b). As demonstrated by Zhou BZ et al. (2020), the viscous correction of a WEC buoy can be almost negligible when its radius to draft ratio is large; the viscous effect on the annular WECs is therefore not considered since all of the WECs used in this study had a large radius to draft ratio. The vector of the system displacement $\boldsymbol{\xi}$ is unknown in the constraint motion equation. By applying the augmentation formulation associated with an unknown Lagrangian multiplier $\boldsymbol{\lambda}$ based on multi-body dynamics (Shabana, 2020), the constrained motion equation can be reformed as

$$\begin{bmatrix}-\omega^2(\boldsymbol{M}+\boldsymbol{a})-\mathrm{i}\omega(\boldsymbol{b}+\boldsymbol{b}_{\mathrm{PTO}}+\boldsymbol{b}_{\mathrm{vis}})+\boldsymbol{k}_{\mathrm{r}}+\boldsymbol{k}_{\mathrm{m}} & \boldsymbol{C}_{\xi}^{\mathrm{T}}\\ -\omega^2\boldsymbol{C}_{\xi} & \boldsymbol{0}\end{bmatrix}\begin{bmatrix}\boldsymbol{\xi}\\ \boldsymbol{\lambda}\end{bmatrix}=\begin{bmatrix}\boldsymbol{F}_{\mathrm{wave}}\\ \boldsymbol{F}_{\mathrm{d}}\end{bmatrix}, \tag{2}$$

where $\boldsymbol{F}_{\mathrm{d}}$ is the generalized force vector associated with the independent coordinates.

The constraint relations of the three annular WECs are identical, denoted as $\boldsymbol{C}(\boldsymbol{\xi})$, and can be expressed as

$$\boldsymbol{C}(\boldsymbol{\xi})=[C_1(\boldsymbol{\xi})\quad C_2(\boldsymbol{\xi})\quad C_3(\boldsymbol{\xi})\quad C_4(\boldsymbol{\xi})\quad C_5(\boldsymbol{\xi})]^{\mathrm{T}}=\boldsymbol{0}, \tag{3}$$

corresponding to the constraints in the five DOFs except for heave. The superscript T represents the transformation of the matrix. $\boldsymbol{C}(\boldsymbol{\xi})$ can be deduced based on the theory of multi-body dynamics. $\boldsymbol{C}_{\xi}$ is the 15×24 linear-constraint Jacobian matrix of $\boldsymbol{C}(\boldsymbol{\xi})$. Letting the first three bodies be the annular WECs and the fourth body be the platform, by assuming small rotational motions of the system and zero Euler angles in the equilibrium position, $\boldsymbol{C}_{\xi}$ can be written in the form of

$$\boldsymbol{C}_{\xi}=\begin{bmatrix}\boldsymbol{C}_{\mathrm{WEC1}} & \boldsymbol{0} & \boldsymbol{0} & \boldsymbol{C}_{\mathrm{platform}}\\ \boldsymbol{0} & \boldsymbol{C}_{\mathrm{WEC2}} & \boldsymbol{0} & \boldsymbol{C}_{\mathrm{platform}}\\ \boldsymbol{0} & \boldsymbol{0} & \boldsymbol{C}_{\mathrm{WEC3}} & \boldsymbol{C}_{\mathrm{platform}}\end{bmatrix}, \tag{4}$$

with

$$\boldsymbol{C}_{\mathrm{WEC}i}=\begin{bmatrix}1 & 0 & 0 & 0 & z_{i0}-z_0 & y_0-y_{i0}\\ 0 & 1 & 0 & z_0-z_{i0} & 0 & x_{i0}-x_0\\ 0 & 0 & 1 & 1 & 0 & 0\\ 0 & 0 & 0 & 0 & 1 & 0\\ 0 & 0 & 0 & 0 & 0 & 1\end{bmatrix}, \tag{5}$$

$$\boldsymbol{C}_{\mathrm{platform}}=\begin{bmatrix}-1 & 0 & 0 & 0 & 0 & 0\\ 0 & -1 & 0 & 0 & 0 & 0\\ 0 & 0 & 0 & -1 & 0 & 0\\ 0 & 0 & 0 & 0 & -1 & 0\\ 0 & 0 & 0 & 0 & 0 & -1\end{bmatrix}, \tag{6}$$

where (x_0, y_0, z_0) is the rotation center of the platform and (x_{i0}, y_{i0}, z_{i0}) is the rotation center of the ith annular WEC (i=1, 2, 3).

The generalized force vector $\boldsymbol{F}_{\rm d}$ associated with the independent coordinates has the form of

$$\boldsymbol{F}_{\rm d}=[\boldsymbol{F}_{\rm d1}^{\rm T} \quad \boldsymbol{F}_{\rm d2}^{\rm T} \quad \boldsymbol{F}_{\rm d3}^{\rm T}]^{\rm T}, \tag{7}$$

with

$$\boldsymbol{F}_{{\rm d}i}=-\omega^2\boldsymbol{C}_{\xi}\boldsymbol{\xi}=\omega^2[x_{i0}-x_0 \quad y_{i0}-y_0 \quad 0 \quad 0 \quad 0]^{\rm T}, \quad i=1,\ 2,\ 3. \tag{8}$$

3.2 Wave-power absorption

The power absorbed by the ith annular WEC $P_i(\omega)$ is

$$P_i(\omega)=\frac{1}{2}\omega^2 b_{\rm PTO}|z_i-z_4|^2, \tag{9}$$

where z_i is the heave motion of the ith annular WEC, and z_4 is the heave motion of the WindFloat platform. The total absorbed wave power $P_{\rm total}(\omega)$ is

$$P_{\rm total}(\omega)=\sum_{i=1}^{3}P_i(\omega). \tag{10}$$

A numerical search method proposed and validated by Zhou et al. (2023b) is employed here to calculate the optimal PTO damping $b_{\rm opt}$ for maximum total wave-power absorption. The corresponding optimal wave power can then be calculated by Eqs. (9) and (10).

The main nomenclature used in this research is given in Table 2.

Table 2 Main nomenclature

Item	Parameter	Symbol
WEC	Outer radius	R
	Inner radius	r
	Draft	d
	Power	P
Wave	General wave frequency	ω
	General wave period	T
	Incident-wave angle	α
	Peak wave period	$T_{\rm p}$

3.3 Validation

The WAFDUT hydrodynamic model and solution method have been long used in the investigation of various offshore structures, and their accuracy has been guaranteed and widely accepted (Zhou BZ et al., 2013; Zhou Y et al., 2020; Cong et al., 2022). We validated the proposed model of the constraint dynamics of the hybrid system by comparing it with the results for a spar-plate device (Fig. 2) from Ruehl et al. (2014). The water depth and wave amplitude were 49.50 and 1.25 m, respectively. The wave periods were 8 and 12 s. Simulations were run with and without PTO damping of 1200 kN·s/m between the float and spar. The comparative results are shown in Fig. 3. The time history of motion was calculated using the amplitude and phase of motion and the results were quite similar.

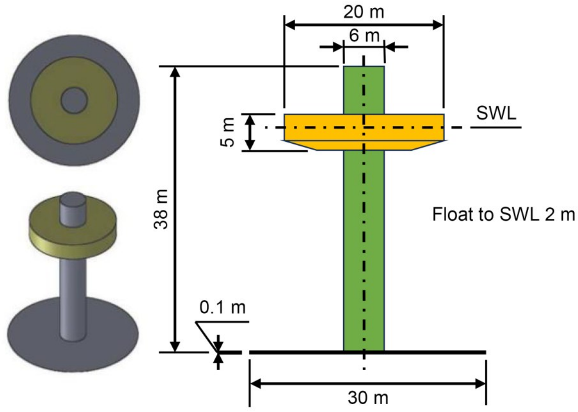

Fig. 2 Sketch of the spar-plate device. SWL is the still water level

4 Numerical results and discussion

The regular incident waves we employed were of unit amplitude. The wave period was from 3 to 25 s with an increment of 0.05 s and the water depth was 325 m.

4.1 Dynamic features of WECs

We investigated the trend of the optimal PTO damping of the annular WECs in the frequency domain, and examined its relationships with the corresponding optimal total wave power and the motion of each annular WEC to (1) reveal the dynamic features of the annular WECs under their optimal conditions and (2) provide a reference for selecting the dimensions of the annular WECs. The incident waves propagated in the positive x-direction (α=0°). In order to make the findings readily generalizable to a wider range of circumstances, we chose the outer radius and draft of a representative annular WEC to be R=11.5 m and d=6.47 m, respectively. The natural period of an annular

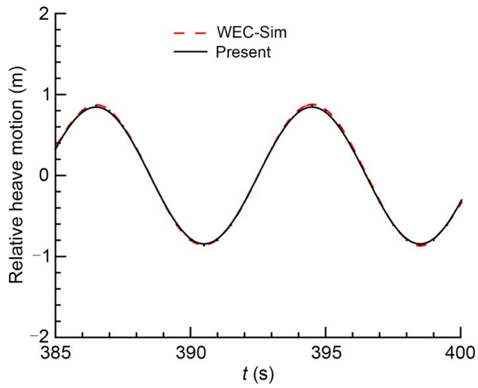

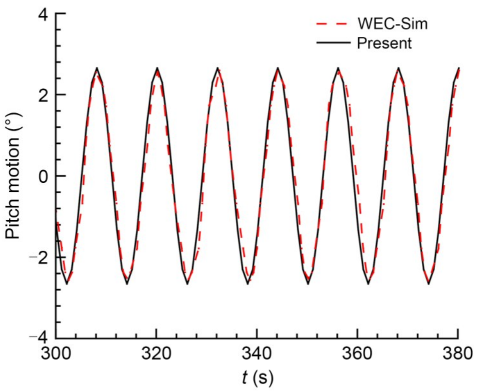

Fig. 3 Comparative results of Wave Energy Converter Simulator (WEC-Sim) and the proposed numerical model: (a) relative heave motion (b_{PTO}=1200 kN·s/m, T=8 s); (b) pitch motion (b_{PTO}=0, T=12 s)

WEC in heave was 7 s. As elaborated in Section 3, the hydrodynamics of the floats were calculated using the WAFDUT numerical package. The constrained dynamics with fluid viscous correction and the wave-power absorption were calculated using an in-house code based on the theory outlined in Section 3. The PTO damping and wave power were optimized with the numerical search method.

The comparative results of the trends for optimal PTO damping and optimal total power are shown in Fig. 4. The tendency of the optimal PTO damping shows a W-shaped pattern. As the wave period increases, it first reaches a local minimum value at T=6.8 s, then a local maximum value at T=10.5 s, and again a local minimum value at T=17.5 s. The tendency of the optimal total wave power shows an M-shaped pattern. The two peaks appear at T=6.8 and 10.2 s, respectively. The first trough of the optimal PTO damping coincides with the first peak of the optimal total wave power, and the peak of the optimal PTO damping coincides

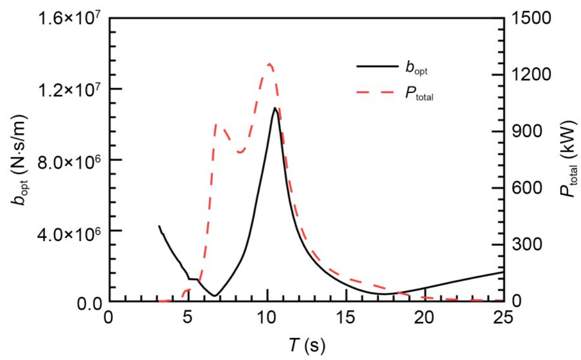

Fig. 4 Optimal PTO damping b_{opt} and optimal total power P_{total}

with the second peak of the optimal total wave power. The second trough of the optimal damping does not show an obvious relationship with any characteristic feature of the optimal total wave power.

The patterns of the optimal PTO damping and optimal total wave power, as well as the matching of peaks and troughs between them, can be seen from a closer examination of the motions of the platform and the annular WECs. The frequency-domain comparative results of the trends of optimal PTO damping, the heave motions of WEC #1 and WEC #2 and the platform, and the relative heave motion between the annular WECs and the platform, are shown in Fig. 5. As WEC #1 and WEC #3 were symmetrically arranged about the x-axis and the waves were normally incident, the results for the two WECs are identical. Comparing Figs. 5a and 5b, although the values of the heave motions of WEC #1 and WEC #2 are quite different within the same wave period, their overall tendencies are similar: two local peaks appear at T=6.8 and 10.5 s, respectively. The differences in the values are because the two WECs were deployed at different places and the local wave heights were influenced by the radiation and diffraction of the platform. Based on this understanding, the formation of the two peaks of the total wave power can be analyzed.

At T=6.8 s, where the first peak occurs, the heave motion of the annular WEC reaches a sharp peak because it is resonant (the deviation from its natural period of 7 s is due to the couplings between the hydrodynamic coefficients of the WEC and those of the platform or those of other WECs). The heave motion of the platform is quite small as it is only weakly excited by the wave. The relative heave motion reaches a sharp local peak due to the large difference in the heave

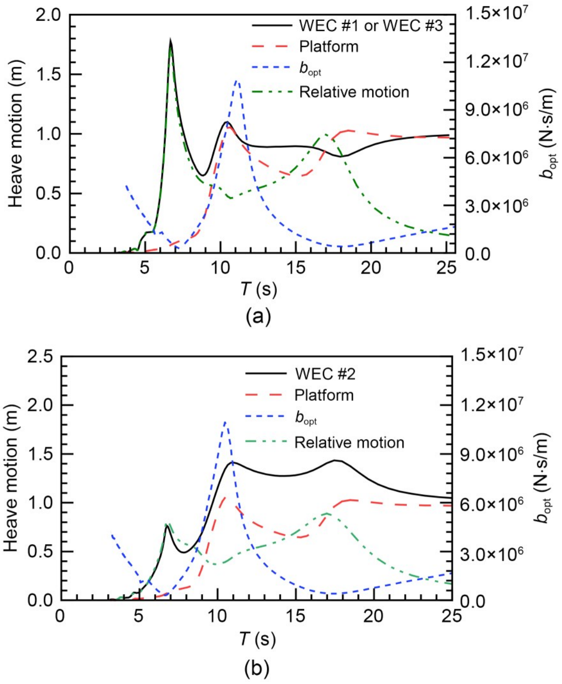

Fig. 5 Optimal PTO damping and dynamic characteristics of the hybrid system: (a) WEC #1 or WEC #3; (b) WEC #2. Only the b_{opt} curve corresponds to the right Y axis

motions between the annular WEC and the platform. The other factor that guarantees the large relative heave motion is the small optimal PTO damping (a local minimum value). It prevents the annular WEC from being lagged by the platform through PTO force. Based on the above analysis, the occurrence mechanism of the first peak of the total wave power can be interpreted as follows. At its natural frequency, the annular WEC resonates and has a much larger heave motion compared with the platform. The small optimal PTO damping guarantees a large relative heave motion between the WEC and the platform. Eq. (9) shows that the total wave power is determined by the product of the relative heave motions and the PTO damping. The combined effect of a large relative heave motion and small PTO damping yields a local peak of the optimal total wave power.

At T=10.5 s, where the second peak of the total wave power occurs, the heave motions of the annular WEC and the platform reach a local peak because they are resonant. The relative heave motion between the two reaches a local trough (for WEC #2, due to the influence of the local wave height determined by the disturbance of the platform, the local trough of the relative heave motion at 9.8 s deviates a bit from T=10.5 s). In this circumstance, the large action and reaction PTO damping forces on the two floating bodies exert a mutual lag effect that reduces the relative heave motion, making the two bodies heave very synchronously in a quasi-resonant state. This situation is analogous to the so-called synchronized mode of a single coaxial-cylinder hybrid system (Jin et al., 2019), but there are some differences. Although a similar phenomenon occurs when the single WEC becomes an array of WECs and all of the WECs move synchronously with the platform, in the synchronized mode, the column and the ring are much more tightly adhered. The reason could be the greater number of WECs and the local wave field associated with each WEC being different, leading to different wave forces on and motions of the WECs. In this case, the synchronization cannot be so complete as when there is only one column and one ring. This situation can be called "sub-synchronization", and the second peak of total wave power it induces can be interpreted as the combined effect of a large optimal PTO damping and small relative heave motion, as in Eq. (9).

At T=18.5 s, the heave motion of the platform reaches a mild peak because it is resonant, but no peak of the total wave power occurs. This is also different from the prediction of Jin et al. (2019) for a single coaxial-cylinder hybrid system, in which a power peak can be obtained. The reasons are as follows. On the one hand, while the platform resonates, its heave motion is not large because it is damped by the heave plates installed beneath the columns. On the other hand, the annular WEC also has a not inconsiderable heave motion due to being excited by long waves. These two effects prevent significant relative heave motion, and the relative heave motion is not necessarily maintained by a large optimal PTO damping. However, the relative heave motion can still reach about 1 m, as shown in Fig. 5. To further interpret the cause of the low total wave power, note that Eq. (9) clarifies that the wave power is also related to the incident-wave frequency ω. In such a long wave with T=18.5 s, wave frequency can be quite small (ω=0.34 rad/s). The combination of the above three effects leads to the disappearance of the possible third peak of the total wave power, even when the platform is resonant.

From the above analysis, it is clear that the regularity found in a single coaxial-cylinder hybrid system cannot be directly applied to a multiple coaxial-cylinder hybrid system due to the additional complexity in the configuration of the hybrid system and the radiated and diffracted local wave field. The first peak of the total wave power linked to the resonance of the annular WEC and the second peak of the total wave power linked to the sub-synchronization of the system can both be used as objectives in tuning the geometry of the annular WECs. An analysis of the influence of the two scenarios on the dynamic features of the platform should be carried out for further evaluation.

The comparative results for platform surge, heave, and pitch motions in the frequency domain with (hybrid system) and without (single platform) integration of annular WECs are shown in Figs. 6a–6c. In Fig. 6a, the trends and values of the surge motions of the single platform and hybrid system are seen to be similar, indicating that the annular WECs have a limited effect on the surge motion of the platform. In Fig. 6b, the heave motion of the single platform is small in the waves from T=3 s to T=14 s. From T=14 s forward, the heave motion of the single platform darts up and reaches a peak of 1.65 m at T=18 s. In the hybrid system, the heave motion of the platform reaches a peak of 1.05 m at T=10.6 s due to stimulation by the large optimal PTO damping, which is much larger than that of the single platform (0.12 m). As the wave period increases, the heave motion of the platform reaches a second peak due to its resonance. The value of the second peak in the hybrid system (1.05 m) is smaller than that for a single platform (1.65 m) due to the lagging effect of the annular WECs. These results indicate that the annular WECs dramatically increase the heave motion of the platform under sub-synchronization but reduce the resonant motion of the platform in the vicinity of its natural frequency. In Fig. 6c, in the hybrid system, it is evident that the pitch motion increases in almost the entire wave-period range. A peak (0.06 rad/s) occurs under sub-synchronization. At the other wave periods, the increases are small. These results indicate that the annular WECs mainly influence the motion of the platform under sub-synchronization conditions, through a large PTO force. With regard to the stability of the platform, this sub-synchronization state should be avoided as it dramatically increases heave and pitch motions, especially the latter, although it helps reduce the resonant motion of the platform at its natural period. The fact that the increase in platform motion occurs in shorter waves that are commonly seen in real seas provides an additional reason to discard sub-synchronization. The first peak of the total wave power due to the resonance of the annular WECs can then be selected as an optimization objective for tuning its dimensions.

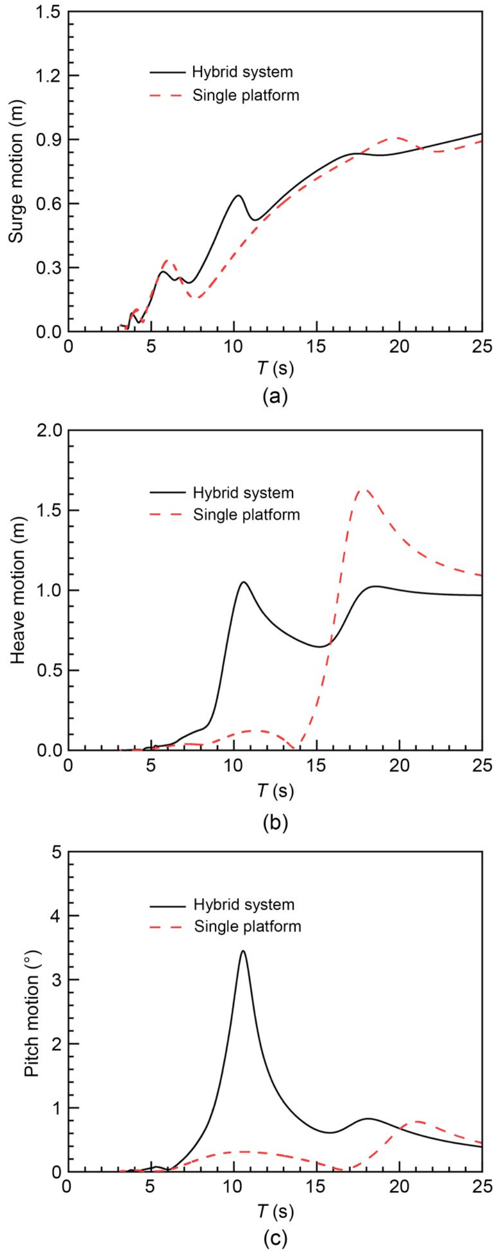

Fig. 6 Motions of the hybrid system and single platform: (a) surge motion; (b) heave motion; (c) pitch motion

4.2 Effect of WEC dimensions

In this section, we discuss optimization of the outer radius and draft of the annular WECs. To make the method and findings more generally applicable, we randomly chose a target operational site in the North Sea as representative. The peak wave period there is T_p=7 s (data from MetOceanView:https://app.metoceanview.com/hindcast-squared/#/). The draft d is obtained by presetting the inner radius to draft ratio r/d. It should be guaranteed that the natural frequency of the annular WEC in the heave mode is T_p. Because tuning the optimal PTO damping according to the immediate wave conditions is difficult to implement even when the most advanced control strategies are applied (Wang et al., 2018, 2020; Sergiienko et al., 2019; Gu et al., 2021), we used a fixed optimal PTO damping obtained under the predominant wave conditions in the representative location (Zhou et al., 2023b) in all the incident waves. Therefore, in the present analysis, for each model of an annular WEC, we used the b_{opt} obtained at T_p=7 s as a universal optimal PTO damping level. The comparative results for total wave power of the annular WECs with r/d=0.80, 0.85, 0.90, and 1.00 are shown in Fig. 7. The detailed dimensions and optimal PTO damping (numerical search) of the four annular WECs are given in Table 3.

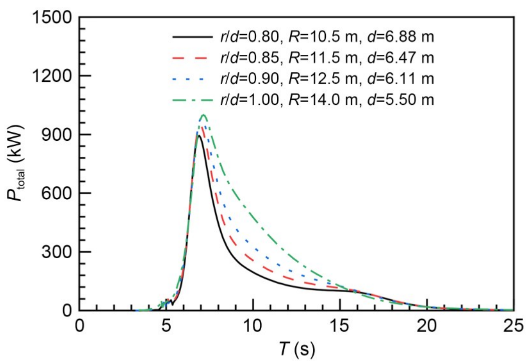

Fig. 7 Influence of WEC dimensions on total power

Table 3 Dimensions and optimal PTO damping of the four annular WECs

r/d	R (m)	r (m)	d (m)	m (kg)	b_{opt} (N·s/m)
0.80	10.5	5.5	6.88	1.77×10^3	4.22×10^5
0.85	11.5	5.5	6.47	2.12×10^3	5.64×10^5
0.90	12.5	5.5	6.11	2.47×10^3	7.35×10^5
1.00	14.0	5.5	5.50	2.93×10^3	1.15×10^6

In Fig. 7, one can see that the general trends of the total wave power of the annular WECs with different r/d ratios are the same: they show a single-peak pattern. In the waves with $T<T_p$, the annular WECs with different r/d ratios absorb almost the same amount of total wave power. At T_p, the total wave power slightly increases as the r/d ratio increases. In the waves with $T_p<T<15$ s, the total wave power of annular WECs with a larger r/d ratio can be much higher than that of WECs with a smaller r/d ratio. From T=15 s on, the annular WECs with different r/d ratios again absorb the same amount of total wave power. Thus, as the inner radius to draft ratio r/d increases, or the annular WECs become flatter, the total wave power in waves longer than the predominant length increases in the operational site, i.e., the wave-power absorption bandwidth expands to the long-wave region.

The surge, heave, and pitch motions of the platform integrated with annular WECs with r/d=0.80, 0.85, 0.90, and 1.00 are shown in Figs. 8a–8c. The motions of a single platform are also given for comparison. Fig. 8a shows that changing the dimensions of the annular WECs in the given range hardly influences the surge motion of the platform. Fig. 8b shows that annular WECs with a larger r/d ratio cause a greater increase of the heave motion in waves from T=3 s to T=16 s and a greater reduction of the heave motion in the vicinity of the natural period of the platform, revealing that a larger lagging effect is created by a flatter annular WEC. However, the difference in the heave motion of the platform between the four hybrid systems is small. Fig. 8c shows that the r/d ratio increases, and that the pitch motion of the platform slightly and gradually increases throughout the most wave-period range.

From Figs. 7 and 8, it is evident that as the inner radius to draft ratio r/d of annular WECs increases, a larger amount of total wave power can be absorbed in a wider wave-period band. The most serious effect is an increase in the pitch motion of the platform, which may affect its dynamic stability. A closer examination of the pitch motions of the hybrid systems with r/d=0.80 and 1.00 shows that the maximum pitch motion increases by 0.29°. The difference between the hybrid system with r/d=1.00 and the single platform is 0.23°. Both of these values are negligible. The total wave power can be further increased by increasing the inner radius to draft ratio r/d of the annular WECs, but two possible circumstances should be mentioned. First, the distance between the columns is a constraint that prevents the outer radius from being larger, since collision between two adjacent WECs cannot be allowed. Second, as the annular WEC becomes too flat, its construction and structural strength can become problematic. Therefore, the radius to draft ratio should be limited

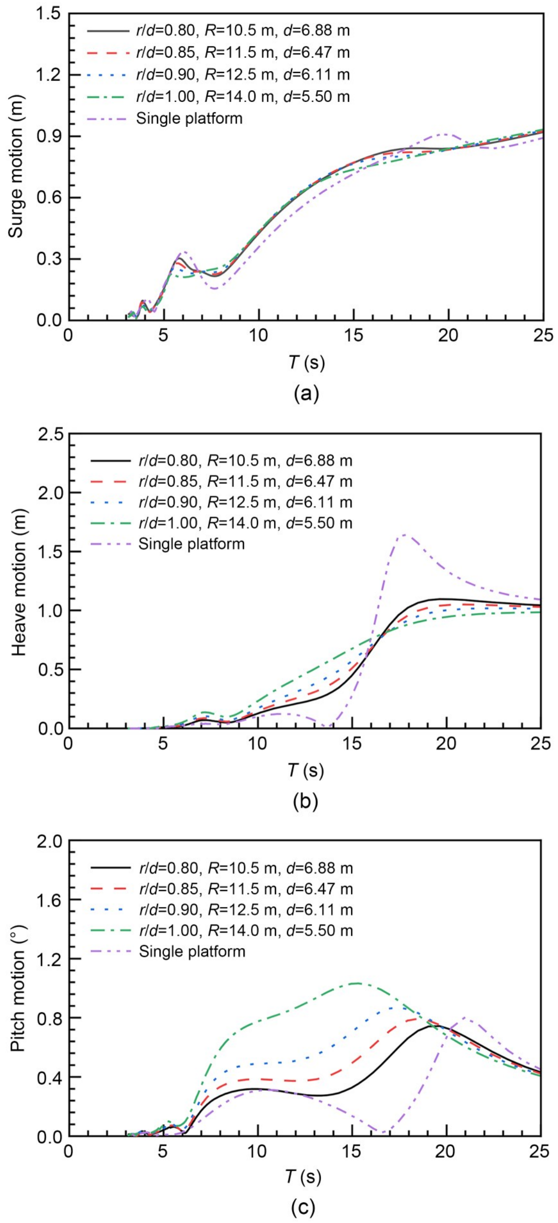

Fig. 8 Influence of WEC dimensions on the motions of the hybrid systems and single platform: (a) surge motion; (b) heave motion; (c) pitch motion

according to the practical installation and manufacturing conditions. In the following analysis, we will use the optimal annular WEC among the four with r/d=1.00.

4.3 Effect of incident-wave angle

We investigated the influence of incident-wave angle on the wave-power absorption and motions of the hybrid system, because in real seas the waves are not always incident in the positive-x direction. The annular WECs discussed here have r/d=1.00, R=14.0 m, and d=5.5 m. The universal optimal PTO damping is fixed at 1.15×10^6 N·s/m.

The total wave power P_{total} and the wave power absorbed by WEC #1, WEC #2, and WEC #3 (P_1, P_2, and P_3) with incident-wave angles α=0°, 90°, and 180° are shown in Figs. 9a–9d. Fig. 9a shows that the single-peak pattern of the total wave power is not affected by variation in the wave direction. The peak power period drifts a bit due to the variation of the local wave field caused by variation in the wave direction. From Figs. 9b–9d, one can deduce that the drift of the peak total wave-power period is mainly caused by the drift of the peak power period of WEC #2, around which the wave field experiences the greatest variation due to changes in wave direction. Fig. 9a also shows that the total wave power has the greatest peak value for α=0° and the broadest band for α=90°. The former is due to the fact that two WECs (WEC #1 and WEC #3) directly face the incident wave and one (WEC #2) is affected by the so-called "shadow effect" when α=0°. The situation is reversed for α=90°. When a WEC is experiencing the shadow effect, the incident-wave energy is absorbed by the WECs in front of it and attenuated by the floating structures in front of it. The number of WECs influenced by the shadow effect is smaller when α=0°; therefore, it has a higher peak power (also evident from the changes in P_1, P_2, and P_3 in Figs. 9b–9d). The latter is due to the particular local wave field disturbed by the platform. From the viewpoint of better power absorption, it is better to avoid the α=180° situation for the platform, i.e., it should not be designed so that only one WEC directly faces the incident-wave train.

The motions of the platform in six DOFs with incident waves where α=0°, 90°, and 180° are shown in Figs. 10a–10f. Fig. 10a demonstrates that for α=90°, the surge motion of the platform almost vanishes, particularly in the long-wave region. The small surge motion in the waves from T=4.5 s to T=16.5 s is induced by the unequal wave excitation forces about the y-axis caused by the asymmetric configuration of the hybrid system. Fig. 10b shows that for α=0° and 180°, the sway motion of the platform vanishes because the hybrid system is symmetric about the x-axis. A comparison between Figs. 10a and 10b shows that the tendencies and values of the surge motions for α=0° and 180° and the sway motion for α=90° are almost equal. This indicates that the oscillating motions of the hybrid

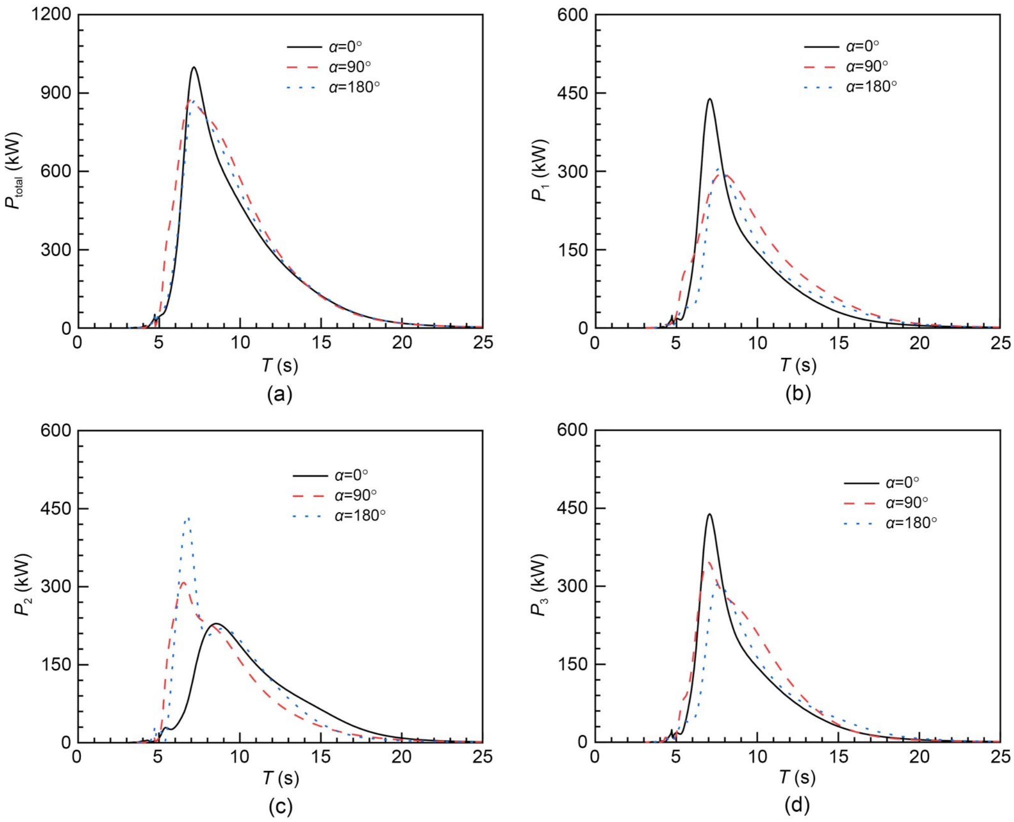

Fig. 9 Influence of incident-wave angle α on the power performance of the hybrid system: (a) P_{total}; (b) P_1; (c) P_2; (d) P_3

system along the wave direction are affected very little by the axis-asymmetric configuration of the hybrid system. Fig. 10c shows that the heave motion of the platform is hardly affected by variations in wave direction. Fig. 10e illustrates that when the wave angle changes from α=0° or 180° to α=90°, the pitch motion can be reduced. The wave force on WECs is more balanced in the x-direction for α=90° than for the other two angles, which produces a lesser fluctuation of the wave torque in pitch. Figs. 10d and 10f show that for α=90°, additional motions in roll and yaw are produced due to the asymmetric configuration of the hybrid system. Compared with the other two angles, the overall effects of an incidence oblique to the x-axis are produced by additional motion in yaw and the direction perpendicular to the wave direction. The former effect may put a slight burden on the servo system, since the maximum yaw angle is about 0.4° and the direction of the nacelle will always be under adjustment. The latter effect has little negative influence on the stability of the hybrid system since the additional motion is quite small.

5 Conclusions

In this study, we proposed a novel hybrid system consisting of a WindFloat platform and three annular, sliding WECs, one on each of its columns. The wave-structure interactions were simulated using a WAFDUT package developed by the Dalian University of Technology. The constrained dynamics of the hybrid system were solved and optimal PTO damping was obtained through a numerical search for maximum power absorption. The dynamic and power absorption features of the annular WECs were investigated and the geometry of the annular WECs was optimized based on a dimensionless method. In addition, the influence of incident-wave direction on the optimized hybrid system was studied. The major conclusions are as follows:

(1) There are two peaks of the total wave power. One is caused by the resonant heave motion of the annular WECs, and the other is obtained under sub-synchronization conditions where the heave motions of the annular WECs and the platform are partly synchronized by the mutual lagging effect caused by a

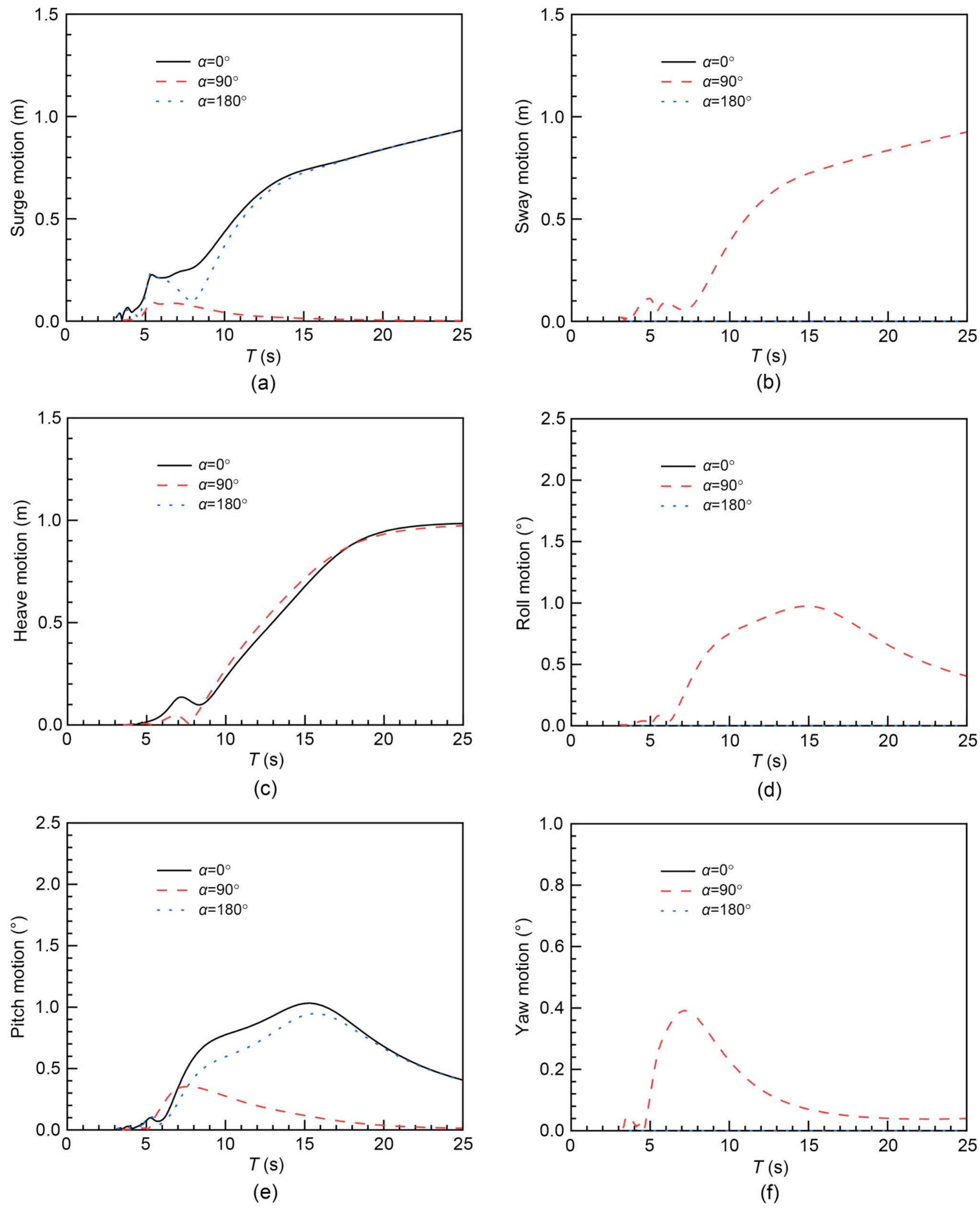

Fig. 10 Influence of incident-wave angle α on the motions of the platform in six DOFs: (a) surge motion; (b) sway motion; (c) heave motion; (d) roll motion; (e) pitch motion; (f) yaw motion

very large PTO damping. Findings based on a single coaxial-cylinder hybrid system cannot be directly applied to this multiple coaxial-cylinder hybrid system due to the complexity of the configuration of the proposed hybrid system and the wave field disturbed by the platform.

(2) The peak of the total wave power produced by resonant heave motion of the annular WECs is most suitable for optimizing the geometry of the annular WECs as it does not damage the dynamic stability of the platform. We found that among the candidate scenarios, a flatter WEC absorbed more power in a wider period range than a slimmer annular WEC, despite it giving slightly more stimulation to the platform motion. However, practically speaking, the annular WEC cannot be made too flat due to limitations in installation and structural strength.

(3) When deploying the hybrid system, it is better to let the side with two WECs face the incident waves rather than single WEC. When the incident-wave

direction does not coincide with the axis of symmetry of the hybrid system, a small additional yaw motion and a small motion along the direction perpendicular to the wave direction will be produced due to the asymmetric configuration of the hybrid system. The overall effect is a small increment in the motion of the hybrid system, which may be negligible.

The application of these findings may have limitations due to the assumptions and idealizations employed. The investigation was carried out using numerical simulations in linear regular waves, based on potential flow theory. It does not consider all real-world physical phenomena that would affect the hybrid floating wind-wave system.

Acknowledgments

This work is supported by the National Natural Science Foundation of China (Nos. 52201322, 52222109, and 52071096), the Guangdong Basic and Applied Basic Research Foundation (Nos. 2022B1515020036 and 2023A1515012144), and the Natural Science Foundation of Guangzhou City (No. 202201010055), China.

Author contributions

Binzhen ZHOU designed the research. Yu WANG and Zhi ZHENG processed the corresponding data. Yu WANG wrote the first draft of the manuscript. Peng JIN and Lei WANG helped to organize the manuscript. Peng JIN and Yujia WEI revised and edited the final version.

Conflict of interest

Binzhen ZHOU, Yu WANG, Zhi ZHENG, Peng JIN, Lei WANG, and Yujia WEI declare that they have no conflict of interest.

References

Chen XP, Wang KM, Zhang ZH, et al., 2017. An assessment of wind and wave climate as potential sources of renewable energy in the nearshore Shenzhen coastal zone of the South China Sea. *Energy*, 134:789-801. https://doi.org/10.1016/j.energy.2017.06.043

Cheng ZS, Wen TR, Ong MC, et al., 2019. Power performance and dynamic responses of a combined floating vertical axis wind turbine and wave energy converter concept. *Energy*, 171:190-204. https://doi.org/10.1016/j.energy.2018.12.157

Clemente D, Rosa-Santos P, Taveira-Pinto F, 2021. On the potential synergies and applications of wave energy converters: a review. *Renewable and Sustainable Energy Reviews*, 135: 110162. https://doi.org/10.1016/j.rser.2020.110162

Cong PW, Teng B, Liu YY, et al., 2022. A numerical approach for hydrodynamic performance evaluation of multi-degree-of-freedom floating oscillating water column (OWC) devices. *Journal of Fluids and Structures*, 114:103730. https://doi.org/10.1016/j.jfluidstructs.2022.103730

Faiz J, Nematsaberi A, 2017. Linear electrical generator topologies for direct-drive marine wave energy conversion–an overview. *IET Renewable Power Generation*, 11(9):1163-1176. https://doi.org/10.1049/iet-rpg.2016.0726

Gaspar JF, Kamarlouei M, Thiebaut F, et al., 2021. Compensation of a hybrid platform dynamics using wave energy converters in different sea state conditions. *Renewable Energy*, 177:871-883. https://doi.org/10.1016/j.renene.2021.05.096

Ghafari HR, Ghassemi H, He GH, 2021. Numerical study of the Wavestar wave energy converter with multi-point-absorber around DeepCwind semisubmersible floating platform. *Ocean Engineering*, 232:109177. https://doi.org/10.1016/j.oceaneng.2021.109177

Gu YF, Ding BY, Sergiienko NY, et al., 2021. Power maximising control of a heaving point absorber wave energy converter. *IET Renewable Power Generation*, 15(14):3296-3308. https://doi.org/10.1049/rpg2.12252

He F, Huang ZH, Law AWK, 2013. An experimental study of a floating breakwater with asymmetric pneumatic chambers for wave energy extraction. *Applied Energy*, 106: 222-231. https://doi.org/10.1016/j.apenergy.2013.01.013

He F, Zhang HS, Zhao JJ, et al., 2019. Hydrodynamic performance of a pile-supported OWC breakwater: an analytical study. *Applied Ocean Research*, 88:326-340. https://doi.org/10.1016/j.apor.2019.03.022

He F, Lin Y, Pan JP, et al., 2023. Experimental investigation of vortex evolution around oscillating water column wave energy converter using particle image velocimetry. *Physics of Fluids*, 35(1):015151. https://doi.org/10.1063/5.0135927

Jeffrey H, Sedgwick J, 2011. ORECCA European Offshore Renewable Energy Roadmap. ORECCA (Offshore Renewable Energy Conversion platforms Coordination Action) Project. http://www.orecca.eu/roadmap_full

Jensen JJ, Mansour AE, 2006. Extreme motion predictions for deepwater TLP floaters for offshore wind turbines. Proceedings of the 4th International Conference on Hydroelasticity in Marine Technology, p.361-367.

Jin P, Zhou BZ, Göteman M, et al., 2019. Performance optimization of a coaxial-cylinder wave energy converter. *Energy*, 174:450-459. https://doi.org/10.1016/j.energy.2019.02.189

Joensen S, Jensen JJ, Mansour AE, 2007. Extreme value predictions for wave- and wind-induced loads on floating offshore wind turbines using FORM. Proceedings of the 10th International Symposium on Practical Design of Ships and Other Floating Structures, p.1158-1166.

Jonkman J, Sclavounos P, 2006. Development of fully coupled aeroelastic and hydrodynamic models for offshore

wind turbines. Proceedings of the 44th AIAA Aerospace Sciences Meeting and Exhibit, p.995.
https://doi.org/10.2514/6.2006-995

Kamarlouei M, Gaspar JF, Calvario M, et al., 2020. Experimental analysis of wave energy converters concentrically attached on a floating offshore platform. *Renewable Energy*, 152:1171-1185.
https://doi.org/10.1016/j.renene.2020.01.078

Lerch M, De-Prada-Gil M, Molins C, 2019. The influence of different wind and wave conditions on the energy yield and downtime of a spar-buoy floating wind turbine. *Renewable Energy*, 136:1-14.
https://doi.org/10.1016/j.renene.2018.12.096

Lu SY, Jason CS, Wesnigk J, et al., 2014. Environmental aspects of designing multi-purpose offshore platforms in the scope of the FP7 TROPOS Project. Proceedings of OCEANS 2014-TAIPEI, p.1-8.
https://doi.org/10.1109/OCEANS-TAIPEI.2014.6964306

Masciola M, Jonkman J, Robertson A, 2014. Extending the capabilities of the mooring analysis program: a survey of dynamic mooring line theories for integration into FAST. Proceedings of the ASME 33rd International Conference on Ocean, Offshore and Arctic Engineering.
https://doi.org/10.1115/OMAE2014-23508

Muliawan MJ, Karimirad M, Moan T, et al., 2012. STC (spar-torus combination): a combined spar-type floating wind turbine and large point absorber floating wave energy converter—promising and challenging. Proceedings of the ASME 31st International Conference on Ocean, Offshore and Arctic Engineering, p.667-676.
https://doi.org/10.1115/OMAE2012-84272

Muliawan MJ, Gao Z, Moan T, et al., 2013. Analysis of a two-body floating wave energy converter with particular focus on the effects of power take-off and mooring systems on energy capture. *Journal of Offshore Mechanics and Arctic Engineering*, 135(3):031902.
http://dx.doi.org/10.1115/1.4023796

Penalba M, Ringwood JV, 2019. A high-fidelity wave-to-wire model for wave energy converters. *Renewable Energy*, 134: 367-378.
https://doi.org/10.1016/j.renene.2018.11.040

Ren NX, Zhang C, Magee AR, et al., 2019. Hydrodynamic analysis of a modular multi-purpose floating structure system with different outermost connector types. *Ocean Engineering*, 176:158-168.
https://doi.org/10.1016/j.oceaneng.2019.02.052

Ren NX, Ma Z, Shan BH, et al., 2020. Experimental and numerical study of dynamic responses of a new combined TLP type floating wind turbine and a wave energy converter under operational conditions. *Renewable Energy*, 151:966-974.
https://doi.org/10.1016/j.renene.2019.11.095

Roddier D, Cermelli C, Aubault A, et al., 2010. WindFloat: a floating foundation for offshore wind turbines. *Journal of Renewable and Sustainable Energy*, 2(3):033104.
https://doi.org/10.1063/1.3435339

Ruehl K, Michelen C, Kanner S, et al., 2014. Preliminary verification and validation of WEC-Sim, an open-source wave energy conversion design tool. Proceedings of the ASME 33rd International Conference on Ocean, Offshore and Arctic Engineering.
https://doi.org/10.1115/OMAE2014-24312

Said HA, Ringwood JV, 2021. Grid integration aspects of wave energy—overview and perspectives. *IET Renewable Power Generation*, 15(14):3045-3064.
https://doi.org/10.1049/rpg2.12179

Sergiienko NY, Cazzolato BS, Arjomandi M, et al., 2019. Considerations on the control design for a three-tether wave energy converter. *Ocean Engineering*, 183:469-477.
https://doi.org/10.1016/j.oceaneng.2019.04.053

Shabana AA, 2020. Dynamics of Multibody Systems. 5th Edition. Cambridge University Press, Cambridge, UK.

Si YL, Chen Z, Zeng WJ, et al., 2021. The influence of power-take-off control on the dynamic response and power output of combined semi-submersible floating wind turbine and point-absorber wave energy converters. *Ocean Engineering*, 227:108835.
https://doi.org/10.1016/j.oceaneng.2021.108835

Teng B, Taylor RE, 1995. New higher-order boundary element methods for wave diffraction/radiation. *Applied Ocean Research*, 17(2):71-77.
https://doi.org/10.1016/0141-1187(95)00007-N

Wan L, Gao Z, Moan T, et al., 2016. Experimental and numerical comparisons of hydrodynamic responses for a combined wind and wave energy converter concept under operational conditions. *Renewable Energy*, 93:87-100.
https://doi.org/10.1016/j.renene.2016.01.087

Wan L, Ren NX, Zhang PY, 2020. Numerical investigation on the dynamic responses of three integrated concepts of offshore wind and wave energy converter. *Ocean Engineering*, 217:107896.
https://doi.org/10.1016/j.oceaneng.2020.107896

Wang L, Ding KLX, Zhou BZ, et al., 2023. Nonlinear statistical characteristics of the multi-directional waves with equivalent energy. *Physics of Fluids*, 35(8):087101.
https://doi.org/10.1063/5.0160775

Wang LG, Isberg J, Tedeschi E, 2018. Review of control strategies for wave energy conversion systems and their validation: the wave-to-wire approach. *Renewable and Sustainable Energy Reviews*, 81:366-379.
https://doi.org/10.1016/j.rser.2017.06.074

Wang LG, Lin MF, Tedeschi E, et al., 2020. Improving electric power generation of a standalone wave energy converter via optimal electric load control. *Energy*, 211:118945.
https://doi.org/10.1016/j.energy.2020.118945

Wu XN, Hu Y, Li Y, et al., 2019. Foundations of offshore wind turbines: a review. *Renewable and Sustainable Energy Reviews*, 104:379-393.
https://doi.org/10.1016/j.rser.2019.01.012

Zhang HM, Zhou BZ, Vogel C, et al., 2020a. Hydrodynamic performance of a floating breakwater as an oscillating-buoy type wave energy converter. *Applied Energy*, 257: 113996.
https://doi.org/10.1016/j.apenergy.2019.113996

Zhang HM, Zhou BZ, Vogel C, et al., 2020b. Hydrodynamic performance of a dual-floater hybrid system combining a floating breakwater and an oscillating-buoy type wave energy converter. *Applied Energy*, 259:114212. https://doi.org/10.1016/j.apenergy.2019.114212

Zhang HM, Zhou BZ, Zang J, et al., 2021a. Effects of narrow gap wave resonance on a dual-floater WEC-breakwater hybrid system. *Ocean Engineering*, 225:108762. https://doi.org/10.1016/j.oceaneng.2021.108762

Zhang HM, Zhou BZ, Zang J, et al., 2021b. Optimization of a three-dimensional hybrid system combining a floating breakwater and a wave energy converter array. *Energy Conversion and Management*, 247:114717. https://doi.org/10.1016/j.enconman.2021.114717

Zhang YX, Zhao YJ, Sun W, et al., 2021. Ocean wave energy converters: technical principle, device realization, and performance evaluation. *Renewable and Sustainable Energy Reviews*, 141:110764. https://doi.org/10.1016/j.rser.2021.110764

Zhou BZ, Ning DZ, Teng B, et al., 2013. Numerical investigation of wave radiation by a vertical cylinder using a fully nonlinear HOBEM. *Ocean Engineering*, 70:1-13. https://doi.org/10.1016/j.oceaneng.2013.04.019

Zhou BZ, Hu JJ, Sun K, et al., 2020. Motion response and energy conversion performance of a heaving point absorber wave energy converter. *Frontiers in Energy Research*, 8:553295. https://doi.org/10.3389/fenrg.2020.553295

Zhou BZ, Zhang Q, Jin P, et al., 2022a. Geometric asymmetry in the energy conversion and wave attenuation of a power-take-off-integrated floating breakwater. *Ocean Engineering*, 246:110576. https://doi.org/10.1016/j.oceaneng.2022.110576

Zhou BZ, Zheng Z, Jin P, et al., 2022b. Wave attenuation and focusing performance of parallel twin parabolic arc floating breakwaters. *Energy*, 260:125164. https://doi.org/10.1016/j.energy.2022.125164

Zhou BZ, Ding KLX, Wang JH, et al., 2023a. Experimental study on the interactions between wave groups in double-wave-group focusing. *Physics of Fluids*, 35(3):037118. https://doi.org/10.1063/5.0142042

Zhou BZ, Hu JJ, Jin P, et al., 2023b. Power performance and motion response of a floating wind platform and multiple heaving wave energy converters hybrid system. *Energy*, 265:126314. https://doi.org/10.1016/j.energy.2022.126314

Zhou BZ, Zheng Z, Jin P, et al., 2023c. Wave attenuation and amplification by an abreast pair of floating parabolic breakwaters. *Energy*, 271:127077. https://doi.org/10.1016/j.energy.2023.127077

Zhou Y, Ning DZ, Shi W, et al., 2020. Hydrodynamic investigation on an OWC wave energy converter integrated into an offshore wind turbine monopile. *Coastal Engineering*, 162:10373. https://doi.org/10.1016/j.coastaleng.2020.103731